# Control and Operation of Multi-Terminal DC Systems for Integrating Large Offshore Wind Farms

Lie Xu, Liangzhong Yao, Masoud Bazargan, and Barry W. Williams

***Abstract*-- This paper investigates the control and operation of multi-terminal VSC based HVDC transmission system technology for connecting large offshore wind farms over long distance. Dynamic system models for both the grid and wind farm side VSCs are provided. DC grid management and active power sharing among various onshore AC networks are studied. Strategies based on coordinated DC droop characteristics for the onshore grid side converters are proposed, to ensure smooth system operation and proper power sharing. PSCAD/EMTDC simulations for a four-terminal DC system for connecting two wind farms with total power rating of 500 MW to two different AC networks are presented to demonstrate robust performance during wind speed and power variations, and the precise power sharing among the two onshore AC systems. Further tests during large disturbances caused by the trip of one of the wind farms are also provided to validate the proposed control and operation of such multi-terminal HVDC systems.**

***Index Terms*-- Converter, doubly fed induction generator, multi-terminal, HVDC, wind farm.**

## I. Introduction

LARGE offshore wind farms are an important form of future renewable energy generation with a number already planned in Europe and around the world. The integration of such offshore wind farms to the grid over distances of tens, and sometimes hundreds, of kilometers is one of the main challenges facing developers and system operators [1, 2]. High voltage DC (HVDC) transmission systems, based on either VSC or conventional line commutated converter (LCC) technologies, have been identified as an alternative to AC connections with a number of advantages including fully controlled power flow, transmission distance using DC is not affected by cable charging currents, and fewer cables required [3, 4].

HVDC systems based on VSC technology are attractive compared to LCC systems for integrating wind farms due to independent reactive power control, no need for external voltage source and fast system dynamics [3]. DC systems based on point-to-point connection for integration of wind farms have been studied extensively with different types of wind generators being considered, e.g., fixed speed induction generator [4-7], and doubly-fed induction generator (DFIG) [3, 8, 9].

Since VSC based HVDC systems can reverse power without changing the DC voltage polarity, the VSC based multi-terminal (MT) system is simpler than LCC MT systems, which require DC voltage polarity change for power reversal. VSC based MT DC systems have been proposed for transmitting power between conventional AC networks [10] and wind farms based on induction generators [11], DFIG [12], and synchronous generators [13]. However, MT systems considered for connecting wind farms in these studies were limited to only one grid side VSC (GSVSC) [11-13]. A true MT VSC system would involve a number of GSVSCs and therefore the control, operation and management of such multi-input systems are significantly more complex and challenging. In [14], the authors proposed a true MT DC system with 2 GSVSCs with one containing close loop DC voltage regulation and the other using DC droop characteristics.

This paper develops new strategies to control and coordinate multiple GSVSCs and wind farm VSCs (WFVSC) within a MT DC transmission system for connecting large offshore wind farms in order to achieve precise power sharing among the onshore AC systems. The paper is organized as follows. Section II outlines the proposed system and Section III investigates the strategies for controlling and managing the MT DC systems to ensure satisfactory operation and power sharing between different receiving networks. The system models of the GSVSC and WFVSC are illustrated in Section IV, then Section V presents simulation results for a four-terminal DC transmission system to validate the proposed system.

## II. System Outline

Fig. 1 shows the single-line diagram of the proposed MT DC system. The system consists of four terminals with two WFVSCs and two GSVSCs. However, the proposed MT DC system is applicable to any number of terminals and any combination of WFVSCs and GSVSCs. The two wind farms considered here are all based on doubly-fed induction generators (DFIG) and located some distance from each other although other wind turbine technologies such as those based on the permanent magnet generator or induction generator can also be used. As shown in Fig. 1, the four terminals are connected together at one common connection point but again other

L Xu and B.W. Williams are with the Department of Electronic and Electrical Engineering, University of Strathclyde, Glasgow G1 1XW, UK. (email: lie.xu@eee.strath.ac.uk, barry.williams@eee.strath.ac.uk)

L Yao and M Bazargan are with AREVA T&D Technology Centre, St. Leonard Avenue, Stafford, ST17 4LX, UK. (email: liangzhong.yao@areva-td.com, Masoud.Bazargan@areva-td.com)

connection arrangements are also applicable.

The WFVSCs collect energy from the wind farms and convert it from AC to DC. The DC power is then transmitted to the GSVSCs via DC cables. The two WFVSCs also control the AC voltages and frequencies of the two respective wind farm networks. The two GSVSCs convert the DC power back to the respective AC grid according to pre-defined arrangement. In addition, they can also provide reactive power/AC voltage control for the grids connected. This feature can be useful as the grid network at the point of connection is sometimes weak with a low short circuit ratio (SCR). A high frequency filter (HFF) is connected at each VSC output terminal to absorb the high frequency harmonics generated by the converters.

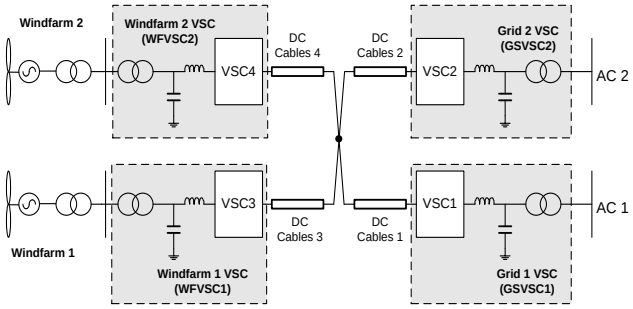


Fig. 1 Single-line diagram of wind farm integration using a MT VSC HVDC system.

## III. Power Sharing and DC Grid Management

For the normal operation of a MT DC system, its common DC link voltage must be closely controlled under all conditions. Abnormal DC link voltage can cause the system to trip and disrupt normal operation. Furthermore, a well-controlled DC voltage indicates balanced active power flow among the multi-terminals. Thus one of the main tasks for the two GSVSCs is to control the DC voltage to ensure the energy collected by the two WFVSCs is transmitted to the grid networks. Furthermore, the transmitted energy has to be distributed between the two grid networks according to pre-defined criteria.

Depending on the different operation arrangements set by the system operators, the two GSVSCs are controlled and operated in different ways. A number of possible operating modes are as follows:

1. One GSVSC (AC system) has priority in terms of transmitting power over the other. Under this arrangement, the second GSVSC will not transmit any power until the capability or the active power order which can come from either system operators or top-level control systems such as AC frequency regulation, of the first GSVSC has been reached.
2. The two GSVSCs (AC systems) each share a certain amount of power being generated by the two wind farms. The power transmission ratio between the two systems can be set and varied by the system operators from time to time.

The first mode has been addressed in [14] and this paper concentrates on the control and operation of the second mode.

As the total power being generated by the wind farms varies from time to time according to the wind speed variation, the total transmitted power of the two GSVSCs also varies. This control mode ensures the power being transmitted by each GSVSC shares a certain ratio which is set and can be varied by system operators.

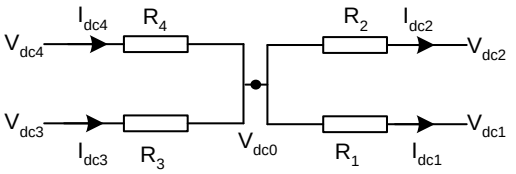


Fig 2 Steady-state DC equivalent circuit of the four-terminal system

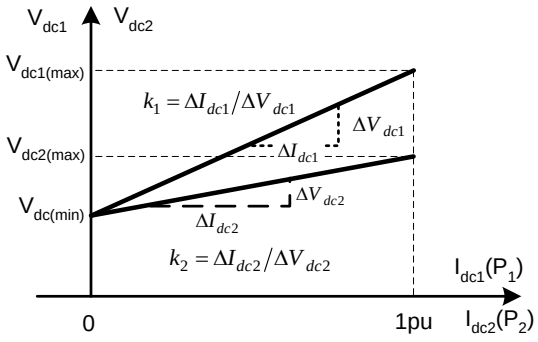


Fig. 3 DC droop characteristics for GSVSC1 and GSVSC2

Fig. 2 shows a simplified steady-state equivalent circuit of the four-terminal DC system where $R_1$-$R_4$ represent the equivalent DC resistances of the four connection cables shown in Fig. 1. $V_{dc1}$-$V_{dc4}$ and $I_{dc1}$-$I_{dc4}$ are the respective DC voltages and currents of the four VSCs. From Fig. 2, the relationship between the two DC voltages at receiving ends, $V_{dc1}$ and $V_{dc2}$ are:

$$\begin{aligned} V_{dc1} &= V_{dc0} - R_1 I_{dc1} \\ V_{dc2} &= V_{dc0} - R_2 I_{dc2} \end{aligned} \tag{1}$$

and

$$V_{dc2} = V_{dc1} + R_1 I_{dc1} - R_2 I_{dc2} \tag{2}$$

where $V_{dc0}$ is the DC voltage at the common DC cable connection point.

Assuming the transmitted power ratio between the two GSVSCs is $n$ and considering the variation of DC voltages are relatively small due to the small cable resistance, there is:

$$\frac{P_1}{P_2} = \frac{V_{dc1} \cdot I_{dc1}}{V_{dc2} \cdot I_{dc2}} \approx \frac{I_{dc1}}{I_{dc2}} = n \tag{3}$$

Fig. 3 shows the DC droop characteristics for the two GSVSCs. The choice of the DC droop characteristic has to take into account the system control and the maximum DC voltage at various terminals considering the ratings for the DC cables and converter equipment. According to Fig. 3, there are:

$$\begin{aligned} I_{dc1} &= k_1 \cdot \Delta V_{dc1} = k_1 \cdot \left(V_{dc1} - V_{dc(\min)}\right) \\ I_{dc2} &= k_2 \cdot \Delta V_{dc2} = k_2 \cdot \left(V_{dc2} - V_{dc(\min)}\right) \end{aligned} \tag{4}$$

Substituting the DC voltages shown in (4) into (2) yields:

$$\frac{I_{dc2}}{k_2} - \frac{I_{dc1}}{k_1} = R_1 I_{dc1} - R_2 I_{dc2} \tag{5}$$

Thus the relationship between the two DC currents is given as

$$\frac{I_{dc1}}{I_{dc2}} = \frac{R_2 + 1/k_2}{R_1 + 1/k_1} = n \tag{6}$$

In order to make sure the transmitted power by the two GSVSCs meet the requirement of (3), according to (6), the relationship between the two droop characteristics is:

$$k_2 = \frac{1}{n/k_1 + n \cdot R_1 - R_2} \tag{7}$$

Thus, if the values of $R_1$ and $R_2$ are know, (7) ensures the ratio of the transmitted power by the two GSVSCs always stays at the required value of *n*. In reality, the real values of $R_1$ and $R_2$ can be different to those used to determine $k_1$ and $k_2$ due to cable temperature variation. Thus, the accuracy of the power distribution can be affected.

According to (6), the impact of the small variations of $R_1$ and $R_2$ on power distribution ratio *n* can be expressed as:

$$\begin{aligned} \Delta n &= \frac{\Delta R_2}{R_1 + 1/k_1} - \frac{R_2 + 1/k_2}{(R_1 + 1/k_1)^2}\Delta R_1 \\ &= \frac{1}{R_1 + 1/k_1}(\Delta R_2 - n \cdot \Delta R_1) \end{aligned} \tag{8}$$

In a practice system, the cable resistance $R_1$ is relatively small compared to $1/k_1$. Thus, according to (8), the smaller $k_1$ is the less impact of cable resistance variation will have on the accuracy of power control. On the other hand, small $k_1$ will results in large DC voltage change during power variation and care must be taken to consider the cable voltage rating and any possible over-voltage during transient conditions.

## IV. VSC Control

### A. GSVSC modeling and control

As the control and operation of GSVSC have been well documented [15, 16], only a brief description is given here. Figs. 4 (a) and (b) show the equivalent AC and DC circuits of the GSVSC, respectively. Referring to Fig. 4(a), the system on the AC side can be expressed in the synchronous d-q reference frame rotating at a speed of $\omega_s$, where the d-axis is fixed to the source voltage $V_s$ and usually determined by a phase-locked loop (PLL), as:

$$\frac{d}{dt}\begin{bmatrix} i_{sd} \\ i_{sq} \end{bmatrix} = [A]\begin{bmatrix} i_{sd} \\ i_{sq} \end{bmatrix} + \frac{1}{L}\begin{bmatrix} -v_{sd} + v_{cd} \\ -v_{sq} + v_{cq} \end{bmatrix} \tag{9}$$

where $[A] = \begin{bmatrix} -R/L & \omega_s \\ -\omega_s & -R/L \end{bmatrix}$.

Using the power balancing equation, the DC side system as shown in Fig. 4(b) is expressed as:

$$P_{ac} = \frac{3}{2}(v_{cd} \cdot i_{sd} + v_{cq} \cdot i_{sq}), \qquad P_{dc} = I_{dc} \cdot V_{dc} \tag{10a}$$

$$I_{dc} \cdot V_{dc} = \frac{3}{2}(v_{cd} \cdot i_{sd} + v_{cq} \cdot i_{sq}) + C\frac{dV_{dc}}{dt} \cdot V_{dc} \tag{10b}$$

Two control loops, i.e., one outer voltage loop and one inner current loop are normally used for the GSVSC. As the design of the current loop is the same as those shown in [15, 16] no more details are giving here.

For the DC voltage loop, as DC droop is used here, the active power order is directly generated from the DC voltage measurement as indicated in (3) and (4). Based on the active power orders, the respective d-axis current references for GSVSC1 and GSVSC2 can be derived as:

$$i_{sd}^{\ *} = \frac{1}{M_d}\left(\frac{4P^*}{3V_{dc}} - M_q \cdot i_{sq}\right) \tag{11}$$

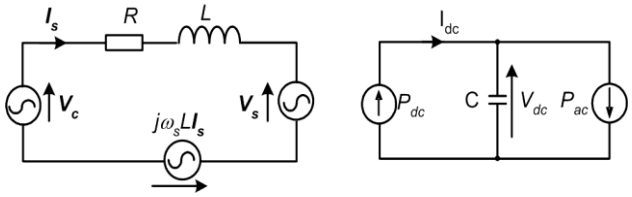


(a) AC (b) DC

Fig. 4 Equivalent circuit of the GSVSC

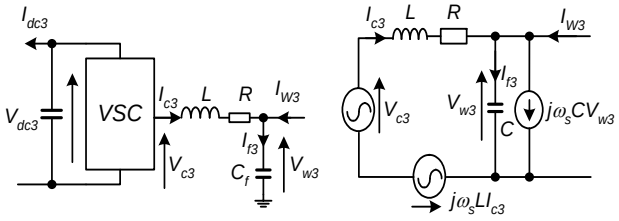


(a) Schematic diagram (b) AC equivalent circuit

Fig. 5 Wind farm side VSC (WFVSC2)

### B. WFVSC modeling and control

The primary aims of the WFVSC are to control the offshore AC voltage amplitude and frequency, and to collect energy generated by the wind farms. Considering the DFIG based wind farm as a controlled current source, Fig. 5 (a) and (b) show the schematic diagram and the AC equivalent circuit of the WFVSC in the d-q synchronous reference frame. The capacitor C as shown in Fig. 5 represents the capacitor in the AC filter as well as part of the AC cable capacitance.

As there is no synchronous generator in the offshore wind farm network, the frequency and phase of the AC voltage are determined solely by the control of the WFVSC. Thus, a PLL circuit is not required and the synchronous speed $\omega_s$ and the d-axis can be set directly by the controller. Based on Fig. 5 (b), the system on the AC side can be expressed in the synchronous d-q reference frame as:

$$\begin{aligned} V_{c3} &= RI_{c3} + L\frac{dI_{c3}}{dt} + j\omega_s LI_{c3} + V_{w3} \\ C_f\frac{dV_{w3}}{dt} &= I_{c3} + I_{w3} - j\omega_s C_f V_{w3} \end{aligned} \tag{12}$$

Separating (12) into d-q components yields a standard state-space model:

$$[\dot{X}] = [A_2][X] + [B_2][U] \tag{13}$$

where

$$[X]=\begin{bmatrix} v_{w3d} \\ v_{w3q} \\ i_{c3d} \\ i_{c3q} \end{bmatrix}, \quad [A_2]=\begin{bmatrix} -1/L & 0 & -R/L & \omega_s \\ 0 & -1/L & -\omega_s & -R/L \\ 0 & \omega_s & 1/C & 0 \\ -\omega_s & 0 & 0 & 1/C \end{bmatrix}$$

and $$[U]=\begin{bmatrix} v_{c3d} \\ v_{c3q} \\ i_{w3d} \\ i_{w3q} \end{bmatrix}, \quad [B_2]=\begin{bmatrix} 1/L & 0 & 0 & 0 \\ 0 & 1/L & 0 & 0 \\ 0 & 0 & 1/C & 0 \\ 0 & 0 & 0 & 1/C \end{bmatrix}$$

The output from the system is the AC voltage on the grid side and can be represented as

$$[Y]=[C][X] \tag{14}$$

where $[Y]=\begin{bmatrix} v_{w3d} \\ v_{w3q} \end{bmatrix}$, $[C]=\begin{bmatrix} 1 & 0 & 0 & 0 \\ 0 & 1 & 0 & 0 \end{bmatrix}$

Fig. 6 shows the block diagram of the wind farm side system including the WFVSC. $G_{ac}(s)$ represents the transfer function of the wind farm AC system and the wind turbines. Based on the system provided in (13) and (14), various techniques such as the pole placement method etc can be used to design a high order control system. Quite often, a control system based on two control loops, i.e., an outer AC voltage loop and an inner current loop are used [14].

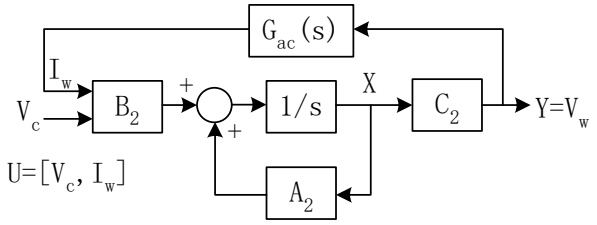


Fig. 6 Block diagram of the offshore system

TABLE I EQUIVALENT PARAMETERS OF THE DC CABLES

| | Cable 1 | Cable 2 | Cable 3 | Cable 4 |
|---|---|---|---|---|
| **DC Resistance** | 1.5Ω | 2.0Ω | 1.5Ω | 2.5Ω |
| **DC Inductance** | 0.02H | 0.02H | 0.02H | 0.025H |
| **DC Capacitance** | 25μF | 15μF | 25μF | 20μF |

## V. SIMULATION STUDIES

Simulation studies of the proposed MT DC system as shown in Fig. 1 for integrating two DFIG based wind farms have been performed using EMTDC/PSCAD. Wind farm 1 (WF1) is rated at 300 MW while wind farm 2 (WF2) is rated at 200 MW. For the grid side, GSVSC1 and GSVSC2 are rated at 300 MW and 200 MW respectively and are connected to separate AC sources with respective SCR of 5 and 7.5. The nominal DC link voltage is 300 kV and the DC characteristics of the four DC cables are listed in Table I.

The two GSVSCs and two WFVSCs are all modeled as 2-level converters switching at 1.5 kHz. DC droop characteristic are implemented for both GSVSCs with $V_{dc(min)}$ set at 1.0pu. For GSVSC1, a DC droop of 20 is used while the DC droop for GSVSC2 is calculated based on the power ratio between the two AC systems using (7).

As previously described, the power outputs from DFIG based wind farms are controlled by their power electronics converters and their operating speeds do not directly affect the dynamic response of the system. Therefore to simplify system modeling, the wind farms are simulated as two lumped DFIG models rated at 300 MW and 200 MW respectively, with parameters shown in the Appendix. The local controller for the DFIG is based on stator flux oriented vector control and the switching frequencies for the converters are 2 kHz. The active power order for the DFIG is generated according to the optimal power-speed curve.

System control and operation with variations of wind speed and power transfer ratio were simulated first and the results are shown in Fig. 7. At the start of the simulation, the initial power transfer ratio for the two GSVSCs is set at 2:1 and the wind speeds are 8m/s and 7m/s for WF1 and WF2 respectively. As can be seen from Fig 7 (d), the generated power are around 100 MW from WF1 and 50 MW from WF2. The total power generated is then transmitted to the onshore AC systems with GSVSC1 and GSVSC2 sharing 97 MW and 49 MW respectively as shown in Fig. 7 (e). This corresponds to a power sharing ratio of 1.98:1. The common DC link is well maintained at all the four converter terminals.

The wind speed for WF2 is increased from 7 m/s to 12 m/s at 1s. The generator at WF2 speeds up and the active power generated starts to increase. This causes the power transmitted to the onshore AC system to increase. As can be seen from fig. 7(e), the power transfer ratio between the two GSVSCs is well maintained during such generation variation and so as the common DC link voltage.

At 3s, the power transfer ratio for GSVSC1 and GSVSC2 is switched from 2:1 to 1:1. As can be seen from Fig. 7 (e), the transmitted powers by the two GSVSCs are quickly changed and equal power sharing is realized in 200ms. It is evident that the operation and response of the system during such switch is very satisfactory.

Again when the wind speed step changed from 8 m/s to 13m/s for WF1, the generated power from WF1 increases and so as the transmitted power by the two GSVSC1s with power ratio maintained at 1:1. At around 4.9s, the maximum power capability of the GSVSC2 (200MW) is reached and its transmitted power cannot be increased. Consequently, the GSVSC1 transmits the remaining active power as can be see from Fig. 7 (e). Again, the DC link voltages at the four converter terminals are well controlled.

Conversely, when the wind speed for WF1 drops from 13 m/s to 7 m/s at 7 s, the DFIG speed, the generated and transmitted active power from WF1 all reduce. Accordingly, GSVSC1 starts to reduce the power transmitted while GSVSC2 remains at 200 MW limit. At 7.2 s, the power being transmitted by GSVSC1 also reduces to 200MW and consequently, GSVSC2 is out of current limit. The total generated power reduces further and so as the power transmitted by the two GSVSCs with their ratio kept constantly at 1:1. Again the system operation is very smooth with no over-voltage/current.

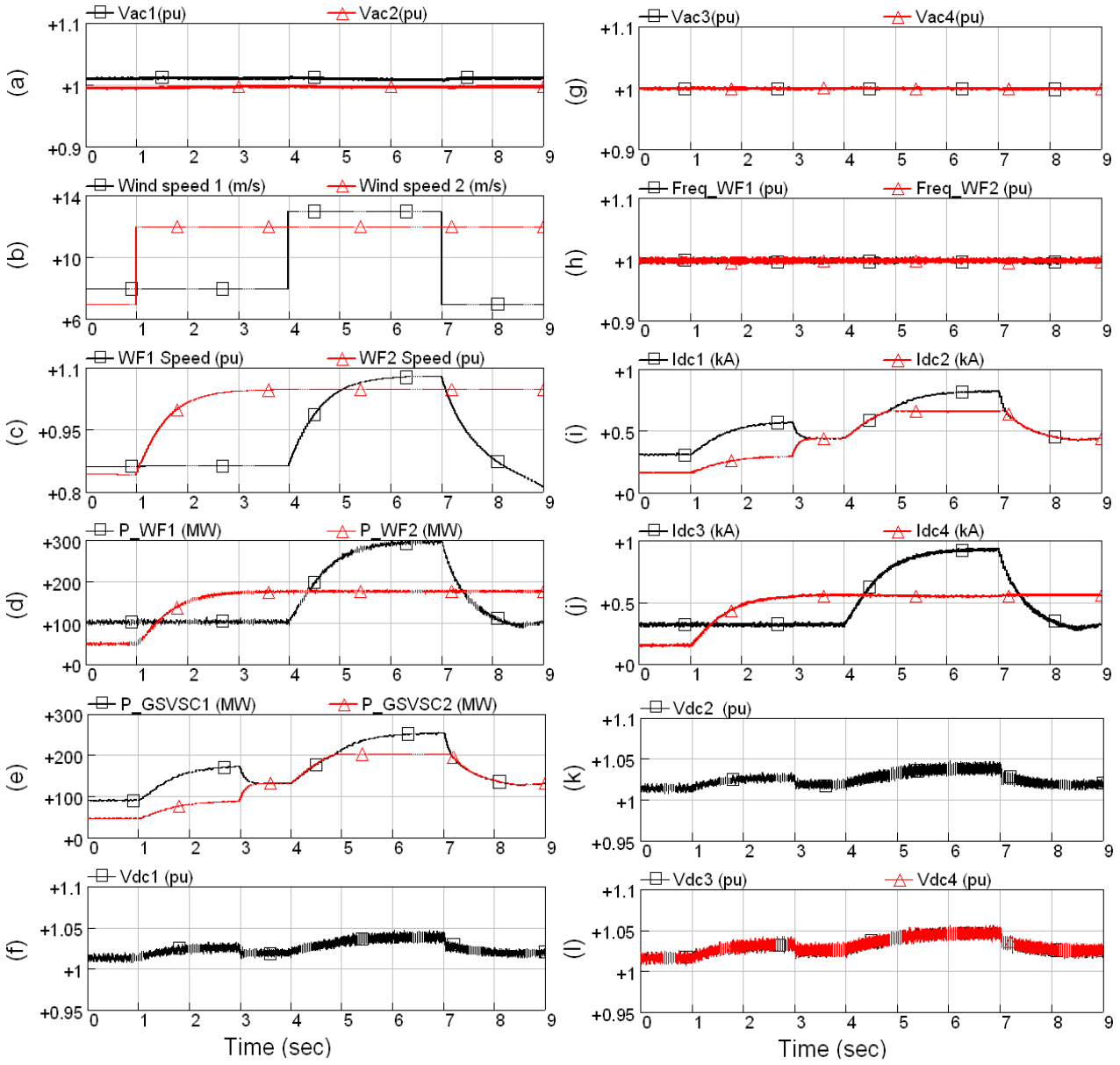


Fig. 7 Simulation results with variation of wind speed: (a) Onshore grid AC voltage; (b) Wind speed; (c) DFIG rotor speed; (d) Power generated by the wind farms; (e) GSVSC1 DC voltage; (f) Power transmitted by the two GSVSC; (g) Offshore AC voltage; (h) Offshore AC frequency; (i) GSVSC DC current; (j) WFVSC DC current; (k) GSVSC2 DC voltage; (l) WFVSC DC voltage.

Further tests on the system control and performance during large disturbance, caused by the trip of WF1 when operated at full power, were carried out and the simulated results are shown in Fig. 8 with the power transmission ratio for the two GSVSCs set at 2:1. The two wind farms are generating 300 MW and 170 MW respectively prior to the trip of WF1 at 7 s, resulting in the sudden loss of 300 MW infeed power. As can be seen in Fig. 8, the loss of 300 MW causes the DC voltage to drop sharply. Consequently, the power transmitted by the two GSVSCs is reduced immediately. As seen in Fig. 8, even under such a severe disturbance, the system continues to operate smoothly in accordance with the pre-defined criteria with the system being well-maintained.

## VI. Conclusions

Integration of large wind farms into transmission networks using a MT VSC based DC system has been studied in this paper. The principles of the proposed system operation and control strategy have been described. Methods for controlling and coordinating the DC grid have been proposed using the coordinated DC droop characteristics based on DC cable resistances to ensure adequate DC voltage control and power sharing among the connected AC grids. Simulation results for a four-terminal system corresponding to wind speed and generation variations have been presented to demonstrate its accurate DC voltage regulation and power sharing. System studies during large disturbance caused by the trip of one wind farm, resulting in the sudden loss of large infeed power, also showed satisfactory performance.

## VII. Appendix

Table II Parameters of the simulated DFIG

| | |
|---|---|
| Stator/rotor turns ratio | 0.3 |
| Stator resistance | 0.0108pu |
| Rotor resistance (referred to the stator) | 0.0121pu |
| Mutual inductance | 3.362pu |
| Stator leakage inductance | 0.102pu |
| Rotor leakage inductance (referred to the stator) | 0.11pu |
| Lumped inertia constant (H) | 1.0 s |

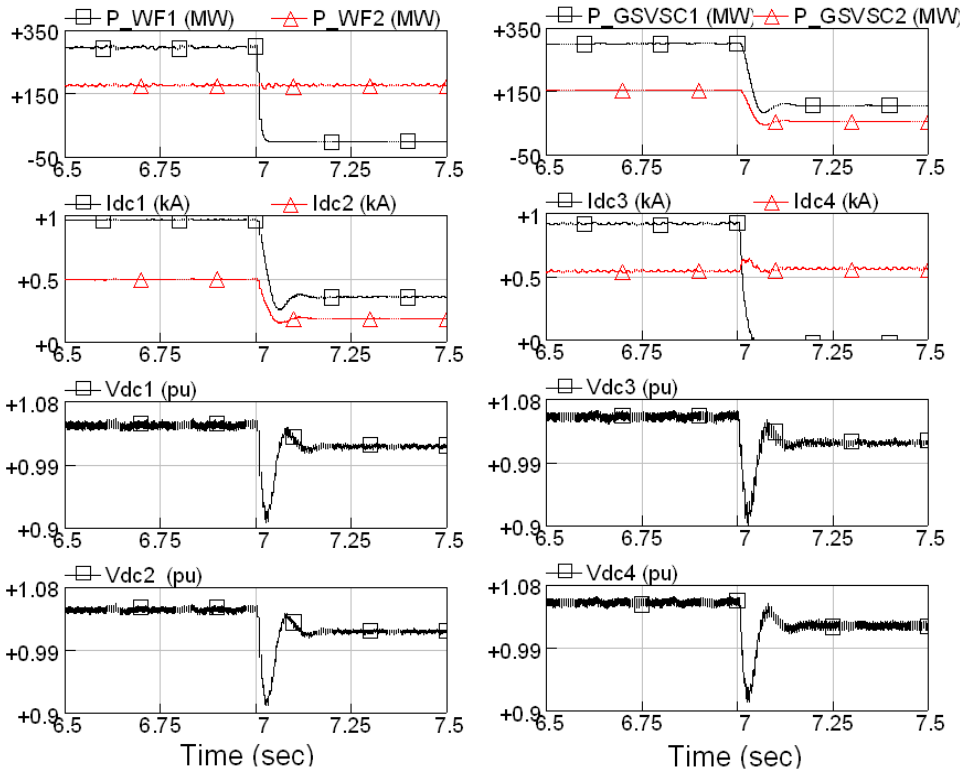


Fig. 8 Simulation results during the disconnection of WF1 with the loss of 300MW infeed power at 7s.

## VIII. References


[1] E. Eriksson, P. Halvarsson, D. Wensky, and M. Hausler, "System Approach on Designing an Offshore Windpower Grid Connection", *Proc. of the 4th International Workshop on Large-Scale Integration of Wind Power and Transmission networks for Offshore Wind Farms*, Sweden, Oct. 2003.

[2] S. M. Bolik, "Grid Requirements Challenges for Wind Turbines", *Proc. of the 4th International Workshop on Large-Scale Integration of Wind Power and Transmission networks for Offshore Wind Farms*, Sweden, Oct. 2003.

[3] L. Xu, and B.R. Andersen, "Grid Connection of Large Offshore Wind Farms using HVDC", *Wind Energy*, Vol. 9, No. 4, July/Aug. 2006. pp. 371-382.

[4] N. Kirby, L. Xu, M. Lucket, and W. Siepmann, "HVDC Transmission for Large offshore Windfarms", *IEE Power Engineering Journal*, June 2002, pp. 135-141.

[5] K.H. Sobrink, P.L. Sorensen, P. Christensen, N. Sandersen, K. Eriksson, and P. Holmberg, "DC Feeder for Connection of a Wind Farm", *Cigre Synposium*, Malaysia, Sept. 1999.

[6] A.K. Skytt, P. Holmberg, and L.E. Juhlin, "HVDC Light for Connection of Wind Farms", *2nd International Workshop on Transmission Networks for Offshore Wind Farms*, Sweden, March 2001.

[7] X. I. Koutiva, T. D. Vrionis, N. A. Vovos, and G. B. Giannakopoulos, "Optimal Integration of an Offshore Wind Farm to a Weak Grid", *IEEE Trans. Power Delivery*, Vol. 21, No. 2, April 2006. pp. 987-994.

[8] D. Xiang, L. Ran, J.R. Bumby, P. Tavner, and S. Yang, "Coordinated Control of an HVDC Link and Doubly fed Induction Generators in a large Offshore Wind Farm", *IEEE Trans. Power Delivery*, Vol. 21, No. 1, Jan. 2006, pp. 463-471.

[9] L. Xu, L.Z. Yao, and C. Sasse, "Grid Integration of Large DFIG based Wind Farms Using VSC Transmission", *IEEE Trans. Power Systems*, Vol. 22, No. 3, Aug. 2007, pp. 976-984.

[10] W. Lu, and B.T. Ooi, "Premium Quality Power Park based on Multi-Terminal HVDC", *IEEE Trans. Power Delivery*, Vol. 20, No. 2, April 2005, pp. 978-983.

[11] W. Lu, and B.T. Ooi, 'Multiterminal LVDC system for optimal acquisition of power in wind-farm using induction generators', *IEEE Transactions on Power Electronics*, Vol. 17, No. 4, July 2002, pp 558 – 563.

[12] L. Jiao, G. Joos, C. Abbey, F. Zhou, and B.T. Ooi, "Multi-terminal DC (MTDC) Systems for Wind Farms Powered by Doubly-Fed Induction Generators (DFIGs), *Proc. of the IEEE PESC*, Aachen, Germany, 2004.

[13] W. Lu, and B.T. Ooi, "Optimal Acquisition and Aggregation of Offshore Wind Power by Multiterminal Voltage-Source HVDC", *IEEE Trans. Power Delivery*, Vol. 18, No. 1, Jan 2003, pp. 201-206.

[14] L. Xu, B. Williams, and L.Z. Yao, "Multi-Terminal DC Transmission Systems for Connecting Large Offshore Wind Farms", *Proc. IEEE PES General Meeting*, Pittsburgh, July 2008.

[15] J. L. Thomas, S. Poullain, and A. Benchaib, "Analysis of a Robust DC-Bus Voltage Control System for a VSC Transmission Scheme", *Proc. of the 7th AC/DC Transmission Conference*, Nov. 2001.

[16] L. Xu, B.R. Andersen, and P. Cartwright, "VSC Transmission System Operating under Unbalanced Network Conditions – Analysis and Control Design", *IEEE Trans. Power Delivery*, Vol. 20, No. 1, Jan. 2005, pp. 427-434.